CO₂ Reduction

Stable Dioxin-Linked Metallophthalocyanine Covalent Organic Frameworks (COFs) as Photo-Coupled Electrocatalysts for CO₂ Reduction

Meng Lu[+], Mi Zhang[+], Chun-Guang Liu[+], Jiang Liu, Lin-Jie Shang, Min Wang, Jia-Nan Chang, Shun-Li Li, and Ya-Qian Lan*

Abstract: *In this work, we rationally designed a series of crystalline and stable dioxin-linked metallophthalocyanine covalent organic frameworks (COFs; MPc-TFPN COF, M = Ni, Co, Zn) under the guidance of reticular chemistry. As a novel single-site catalysts (SSCs), NiPc/CoPc-TFPN COF exhibited outstanding activity and selectivity for electrocatalytic CO₂ reduction (ECR; Faradaic efficiency of CO (FE_{CO}) = 99.8(±1.24) %/ 96.1(±1.25) % for NiPc/CoPc-TFPN COF). More importantly, when coupled with light, the FE_{CO} and current density (j_{CO}) were further improved across the applied potential range (−0.6 to −1.2 V vs. RHE) compared to the dark environment for NiPc-TFPN COF (j_{CO} increased from 14.1 to 17.5 A g⁻¹ at −0.9 V; FE_{CO} reached up to ca. 100 % at −0.8 to −0.9 V). Furthermore, an in-depth mechanism study was established by density functional theory (DFT) simulation and experimental characterization. For the first time, this work explored the application of COFs as photo-coupled electro-catalysts to improve ECR efficiency, which showed the potential of using light-sensitive COFs in the field of electro-catalysis.*

Introduction

The excessive CO₂ emissions have triggered serious climate and environmental problems, especially the green-house effect and sea-level rise.[1] Electrocatalytic CO₂ reduction (ECR) to high-value-added chemicals is an efficient way to utilize CO₂ and mitigate greenhouse gas emissions, also offers opportunities for large-scale and long-term energy storage.[2] Despite many efforts devoted to the electrochem-ical conversion of CO₂, the relatively low efficiency, selectiv-ity and poor stability of CO₂ reduction are still the main obstacles to the further development of ECR.[3] In the field of ECR, except that CO₂ reduction is driven by electric energy solely, the photo-coupled electrocatalytic CO₂ reduction (PECR) method further provides a promising way to realize its high activity.[4] When coupled with photon energy, the light irradiation strongly interferes with the electronic properties of light sensitive electrocatalysts, thus changing the ECR catalytic process and activity.[5] However, the studies in this field are limited and challenging.[5,6] Therefore, it is necessary to design and develop new photo-coupled electrocatalyst system to further explore this novel process. For a PECR catalyst, it demands an efficient combination of electric and light energy, and the following requirements must be met at the same time: 1) possess effective catalytic active site for CO₂ reduction; 2) have efficient light absorption and photo-electron conversion capabilities; 3) have good structural stability when light irradiation and electric energy were simultaneously applied.

Metal-nitrogen-carbon (M-N-C) catalysts, especially met-allo-phthalocyanine based single-site catalysts (SSCs) have been shown to have the ability to activate CO₂.[7] In order to solve the substrate accessibility and chemical stability of these SSCs, a general method is to integrate these single-site molecules with carbon substrates, such as carbon powder, carbon nanotubes, or graphene to form hybrid catalytic materials.[8] However, this hybrid method is still difficult to solve the problem of homogeneity of catalytic sites and much improvement is still needed in their ECR activity and stability.[7d] Assembling single-site molecules into highly ordered crystalline structures would be an ideal way to overcome the above issues.[9] Covalent organic frameworks (COFs), a class of newly developed crystalline materials, which have directional structural designability and high stabilities are a promising platform for SSCs.[9,10] On the other hand, metallophthalocyanine is a photosensitive 18π aromatic macrocyclic compound, in addition to its efficient light absorption capacity, its electronic properties can be greatly changed under light driving.[11] Hence, the phthalo-cyanine-based materials address the basic requirements of photo coupled electrocatalysts for PECR. Therefore, based on the periodic structural features of COFs, assembling metallophthalocyanine molecules into COFs not only ensures highly independent single metal active sites, but also guaran-tees ideal uniform dispersion of them in the whole platform. According to the above, rationally designed crystalline

[*] M. Lu,[+] Dr. J. Liu, L.-J. Shang, M. Wang, J.-N. Chang, Prof. S.-L. Li, Prof. Y.-Q. Lan
Jiangsu Collaborative Innovation Centre of Biomedical Functional Materials, School of Chemistry and Materials Science, Nanjing Normal University
No. 1, Wenyuan Road, Nanjing 210023 (China)
E-mail: yqlan@njnu.edu.cn

M. Zhang[+]
School of Chemistry, South China Normal University
Guangzhou 510006 (P. R. China)

Prof. C.-G. Liu[+]
Department of Chemistry, Faculty of Science, Beihua University
Jilin City 132013 (P. R. China)

[+] These authors contributed equally to this work.

Supporting information and the ORCID identification number(s) for the author(s) of this article can be found under:
https://doi.org/10.1002/anie.202011722.

metallophthalocyanine COFs will be an ideal model for studying and realizing high efficient ECR and further applying to photo coupled electrocatalytic reaction.
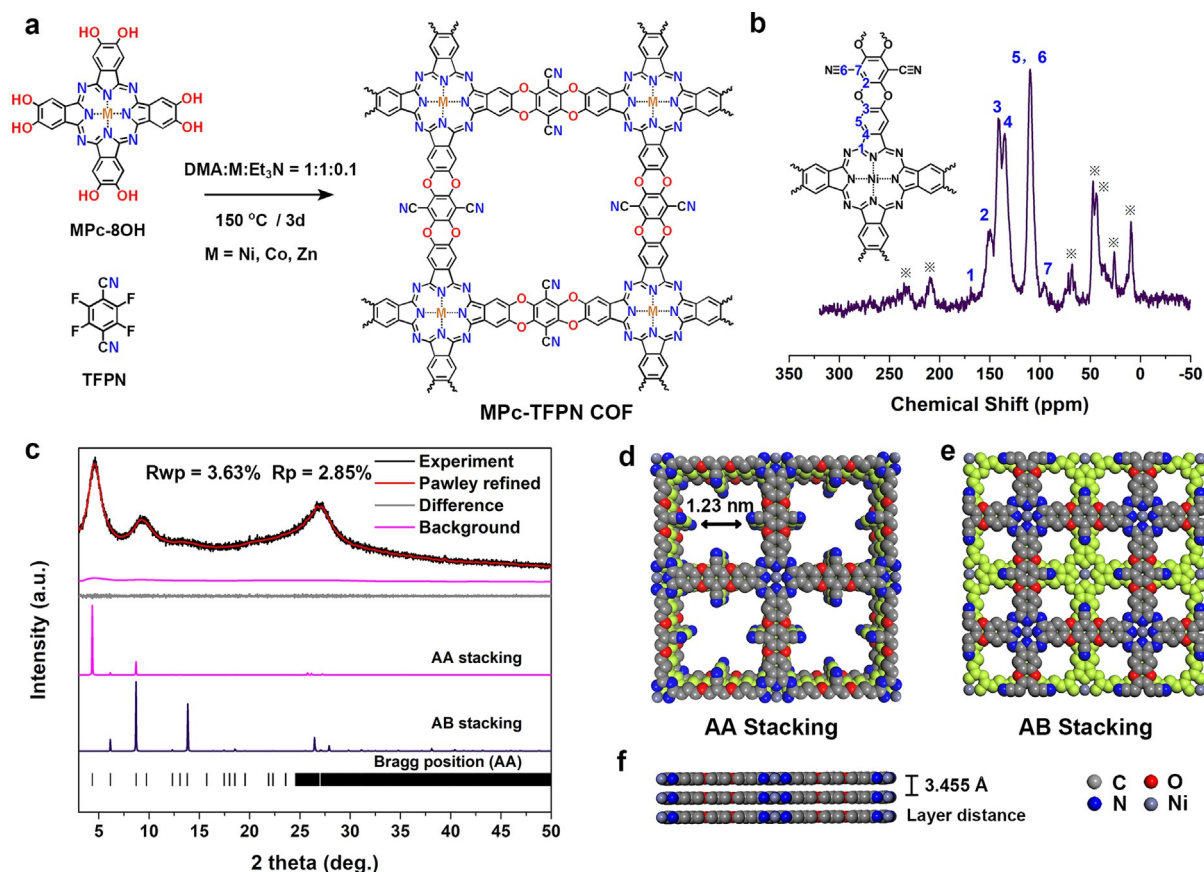
Herein, a series of dioxin-linked crystalline metallophthalocyanine covalent organic frameworks (MPc-TFPN COF, M = Ni, Co, Zn) were first designed and synthesized under the guidance of reticular chemistry. These COFs show high stability and crystallinity even under harsh chemical environments such as concentrated acids and base for at least 1 month. As an exclusive SSCs for ECR, NiPc-TFPN COF and CoPc-TFPN COF exhibited remarkable activity and selectivity for CO$_2$ to CO conversion. The Faradaic efficiency of CO (FE$_{CO}$) up to 99.8($\pm$1.24)% for NiPc-TFPN COF and 96.1($\pm$1.25)% for CoPc-TFPN COF at -0.9 V vs. RHE, respectively, and remarkable cycle stability with neither an obvious current drop (an average of -16.3 mA cm^{-2} for NiPc-TFPN COF and -12.1 mA cm^{-2} for CoPc-TFPN COF) nor large FE fluctuation was observed during 60 h ECR test. More importantly, with the assistance of light, the FE$_{CO}$ and the current density were further enhanced over a wide potential range (-0.6 to -1.2 V vs. RHE) compared to the dark environment for NiPc-TFPN COF (j_{CO} increased from 14.1 to 17.5 mA cm^{-2} at -0.9 V; FE$_{CO}$ reached up to $\approx$100% at -0.8 to -0.9 V, which is one of the highest in reported COFs), suggesting that the coupling of light energy plays an

important role. Besides, density functional theory (DFT) calculations revealed the rate-determining step and activity determining processes on the COFs based-SSCs, and also revealed the mechanistic details of the photo coupled ECR activity and selectivity of this family of catalysts.

Results and Discussion

Synthesis of dioxin-linked metallophthalocyanine COFs

As shown in Figure 1, an aromatic nucleophilic substitution between o-difluorobenzene and catechol under the catalysis of triethylamine (Et$_3$N) was applied to condense 2,3,9,10,16,17,23,24-octahydroxyphthalocyaninato Metal (MPc-8OH, M = Ni, Co, Zn) with tetrafluorophthalonitrile (TFPN) to form three dioxin-linked phthalocyanine COFs, which were denoted as NiPc-TFPN COF, CoPc-TFPN COF and ZnPc-TFPN COF, respectively. The strong electron-withdrawing nitrile groups of TFPN can enhance the electrophilicity of its C–F bond and therefore the reactivity toward MPc-8OH.[12] Highly crystalline MPc-TFPN COF were synthesized through the mixture of MPc-8OH and TFPN in N, N-dimethylacetamide (DMA)/mesitylene (M)/Et$_3$N = 1:1:0.1 (*v:v:v*) at 150°C for 3 days (Figure 1a).

Figure 1. Synthesis and structure of dioxin-linked metallophthalocyanine COFs. a) Schematic of the synthesis and structure of MPc-TFPN COF through the condensation of MPc-8OH and TFPN. b) ^{13}C ssNMR spectrum of NiPc-TFPN COF. c) Experimental, Pawley refined, and simulated PXRD patterns (AA stacking and AB stacking mode) of NiPc-TFPN COF. d) Top view of simulated AA stacking mode and e) AB stacking mode for NiPc-TFPN COF crystal structure. f) Side view of AA stacking mode for NiPc-TFPN COF crystal structure.

The formation of the dioxin linkages in the MPc-TFPN COF were first confirmed by solid state ^{13}C cross-polarization magic angle spinning (ss ^{13}C CP/MAS) NMR spectroscopy and Fourier Transform Infrared Spectroscopy (FTIR). The resonance signals at 141 and 150 ppm in NMR as shown in Figure 1b, which are characteristic of the carbons of C−O and the signal at 95 ppm is assigned to aromatic carbons connected to nitriles, whereas those at 109 and 135 ppm are assigned to the nitrile carbons and aromatic carbons. Similarly, the ^{13}C CP-MAS NMR spectrum of CoPc-TFPN COF and ZnPc-TFPN COF can also be fully assigned (Figures S1,2). The FTIR spectrum revealed stretching vibration bands at 1277 cm^{-1} and 1010 cm^{-1}, which belong to the dioxin C−O asymmetric and symmetric stretching modes (Figures S3–5).[12] All these results confirmed the successful condensation reaction required for the dioxin-linked MPc-TFPN COFs structure.
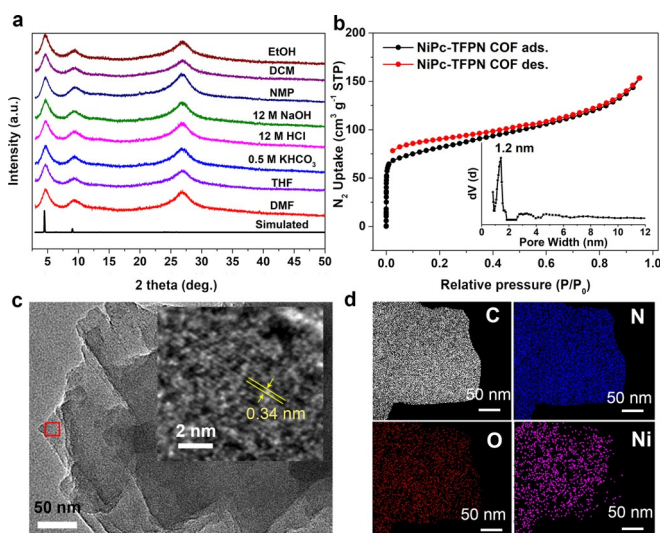
Crystal Structure

The crystal structure of MPc-TFPN COF was determined by the powder X-ray diffraction (PXRD) combined with theoretical structural simulations using Materials Studio package (Figure 1c). The AA (eclipsed) stacking model (Figure 1d) with $P4/mmm$ (No.123) space group based on NiPc-TFPN COF was built and then carried out Pawley refinements of the PXRD patterns for full profile fitting against the proposed models, which provided a unit cell parameter of $a = b = 20.3180$ Å and $c = 3.4545$ Å, $\alpha = \beta = \gamma = 90°$. The calculated PXRD diffraction patterns matched well with the experimental results, with R$wp = 3.63\%$ and R$p = 2.85\%$. The AB (staggered) stacking structure was also simulated (Figure 1e), while the comparison of its PXRD profile with the experimental one showed significant deviations, ruling out the AB stacking model. NiPc-TFPN COF exhibited diffraction peaks at 4.37°, 6.17° and 8.71°, which are assigned to the (100), (110) and (200) planes, respectively. The simulated crystal structure showed the layer distance of NiPc-TFPN COF is 3.455 Å (Figure 1f).

In MPc-TFPN COF, the four nitrogen atoms located in the center of phthalocyanine can coordinate with different metal atoms, thus realizing the modulation of COFs structure at the atomic level. As shown in the PXRD patterns in Figure S6, CoPc/ZnPc-TFPN COF also displayed crystalline structure. The comparison of PXRD patterns of MPc-TFPN COF with those of TFPN and MPc-8OH monomers were also conducted (Figures S7–9), which proved that MPc-TFPN COF has high purity. More details and raw data are given in the Supporting Information. As we know, most of the previously reported phthalocyanine COFs exhibited poor structural chemical stability,[13] while as dioxin-linked phthalocyanine COFs formed from irreversible reactions, MPc-TFPN COFs displayed high thermal and chemical stability. The thermal stabilities of MPc-TFPN COFs were confirmed by thermogravimetric analysis (TGA, Figures S12–17). Take NiPc-TFPN COF as an example, it showed no obvious change up to ≈400°C under nitrogen and ≈300°C under oxygen atmosphere. The chemical stability of NiPc-TFPN COF was examined by immersing it into different solvents (including different commonly used organic solvents such as N-Methyl-2-pyrrolidone (NMP), N, N-dimethylformamide (DMF), tetrahydrofuran (THF), dichloromethane (DCM), ethanol (EtOH) and acid/base such as concentrated HCl (12 M), concentrated NaOH (12 M) and 0.5 M KHCO$_3$)) at room temperature for at least 1 month. No obvious differences were observed from the PXRD after the treatment (Figure 2a), indicating its structural robustness. The porosity of these COFs was assessed by nitrogen sorption measurements at 77.3 K (Figure 2b, Figures S18,19). The measured pore sizes (≈1.2 nm) for NiPc-TFPN COF were consistent with the theoretical results (Figure 2b, inset). The Brunauer-Emmett-Teller (BET) surface area of NiPc-TFPN COF was found to be 252.375 m^{2}g^{-1}. Appreciable amounts of CO$_2$ adsorption on MPc-TFPN COF were observed (Figures S20–22), which should be attributed to not only the combination of microporous character and the heteroatom-rich channels in the MPc-TFPN COF, but also a Lewis acid-base interaction between the coordinated metal ions and absorbed CO$_2$ molecules.[14]

Scanning electron microscopy (SEM) and transmission electron microscopy (TEM) were performed to characterize the morphology of MPc-TFPN COF, which showed that NiPc-TFPN COF was composed of microcrystalline particles with 200–300 nm in diameter (Figures S23–25). The structural characteristics of NiPc-TFPN COF were visualized by high resolution transmission electron microscopy (HRTEM). As shown in Figure 2c, NiPc-TFPN COF displayed clear lattice fringes of (001) crystal face, also confirmed the simulated crystal structure. Energy-dispersive X-ray spectroscopy (EDX) analysis revealed that C, N, O, and Ni are uniformly distributed over NiPc-TFPN COF (Figure 2d). Additionally, from EDX, Co and Zn are also uniformly distributed over CoPc-TFPN COF and ZnPc-TFPN COF (Figures S26,27),
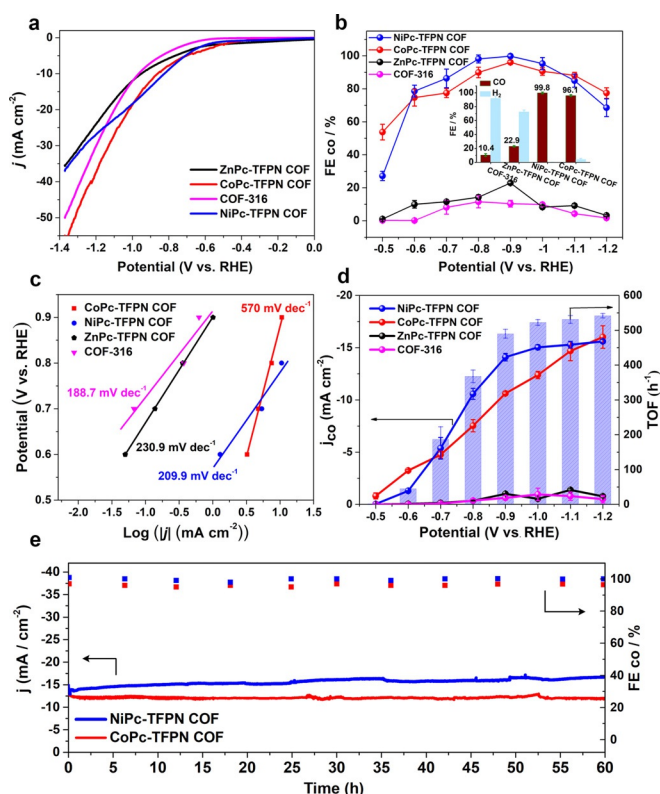

Figure 2. Characterization and morphology of MPc-TFPN COF. a) Chemical stability of NiPc-TFPN COF. b) N$_2$ adsorption isotherm of NiPc-TFPN COF. Inset is the pore size distribution of NiPc-TFPN COF. c) HRTEM image and lattice fringes of NiPc-TFPN COF. d) Element mapping of NiPc-TFPN COF.

respectively. X-ray photoelectron spectroscopy (XPS) was performed to explore the metal valence states in MPc-TFPN COF (Figures S28–33). In the XPS spectrum of Ni 2p for NiPc-TFPN COF, the peaks at 855.7 eV (Ni 2p 3/2) and 873.0 eV (Ni 2p 1/2) correspond to the +2 state of Ni. For CoPc-TFPN COF and ZnPc-TFPN COF, both cobalt and zinc are also divalent from XPS results. The metal content in NiPc-TFPN COF, CoPc-TFPN COF and ZnPc-TFPN COF were determined to be 5.39 wt.%, 5.48 wt.% and 5.08 wt.% respectively by inductively coupled plasma optical emission spectrometry (ICP-OES).

Electrochemical CO_2 reduction activity of COFs

Based on the above illustration of the MPc-TFPN COF crystal structure, it can be seen that MPc-TFPN COF represent highly uniformly dispersed single metal sites (the distance between the two adjacent single metal atoms is 2.03 nm), making these COFs an ideal SSCs for ECR. The ECR activities for NiPc-TFPN COF, CoPc-TFPN COF, ZnPc-TFPN COF and COF-316 were first evaluated, respectively, in a two-compartment H-type cell (separated by Nafion®212) with a CO_2-saturated 0.5 M $KHCO_3$ solution (pH 7.2) as electrolyte in dark environment. In classic ECR experiments, we use current density (j) and faradaic efficiency of the reduction products as the indices to evaluate the performance.[15] As revealed by the linear sweep voltammetry curves (LSV) (Figure 3a), all MPc-TFPN COF has a small onset potential (−0.42 V for CoPc-TFPN COF, −0.48 V for NiPc-TFPN COF and −0.22 V for ZnPc-TFPN COF, versus RHE) on CO_2-saturated 0.5 M $KHCO_3$ solution. Interestingly, at low (< −0.7 V) and high potentials (> −1.1 V), the total current density (j_{total}) of CoPc-TFPN COF is higher than that of NiPc-TFPN COF, while at wide range medium potentials (−0.7 to −1.1 V), NiPc-TFPN COF performs better than CoPc-TFPN COF. In addition to current density, the selectivity in ECR was also investigated. We tested all the COFs under wide potentials ranges from −0.5 V to −1.2 V, and obtained the corresponding FE values (Figure 3b). It was noted that the total FE of CO and H_2 was found to be ≈ 100% over the entire tested potential range, and no other products were detected. Good reproducibility was observed in measurements of three independently prepared samples. Our results showed that both CoPc-TFPN COF and NiPc-TFPN COF exhibited excellent ECR catalytic activity and selectivity. In particular, the maximal FE_{CO} can reach up to 99.8(± 1.24)% with a partial current density (j_{CO}) of ≈ 14.1 mA cm^{-2} (A g^{-1}) at −0.9 V versus RHE (Figure 3b and d) for NiPc-TFPN COF. While as for CoPc-TFPN COF, the maximal FE_{CO} can reach to 96.1(± 1.25)% with a partial current density (j_{CO}) of ≈ 10.6 mA cm^{-2} at the same conditions for NiPc-TFPN COF, which is consistent with other reports of using Co-phthalocyanine as catalyst for ECR.[8a,b,16] However, for contrast samples, COF-316 (without metal phthalocyanine but with TFPN unit, also known as JUC-505, Figure S11)[12] and ZnPc-TFPN COF only showed relatively low catalytic efficiency (FE_{CO} = 10.4% and 22.9% for COF-316 and ZnPc-TFPN COF, respectively) (Figure 3b, inset). The ECR

Figure 3. Electrocatalytic CO_2 reduction performances of MPc-TFPN COF. a) LSV curves for the MPc-TFPN COF and contrast catalysts. b) The Faradic efficiency of carbon monoxide calculated overpotential range from −0.5 to −1.2 V. Inset is the FE_{CO} and FE_{H_2} of different COFs. c) Tafel plots. d) Partial CO current density and TOF (h^{-1}). e) Stability of NiPc-TFPN COF and CoPc-TFPN COF at −0.9 V versus RHE. The error bars represent the standard deviation of three independent measurements. All the tests were conducted in a CO_2-saturated 0.5 M $KHCO_3$ aqueous solution under dark environment.

activity of MPc-8OH monomers was also tested (Figures S34–36), while the highest FE_{CO} of them only reaching ≈ 85% due to the sluggish diffusion of CO_2. These results show that the crystalline structure of COFs and its metal-lophthalocyanine as SSCs are particularly important for CO_2 reduction.
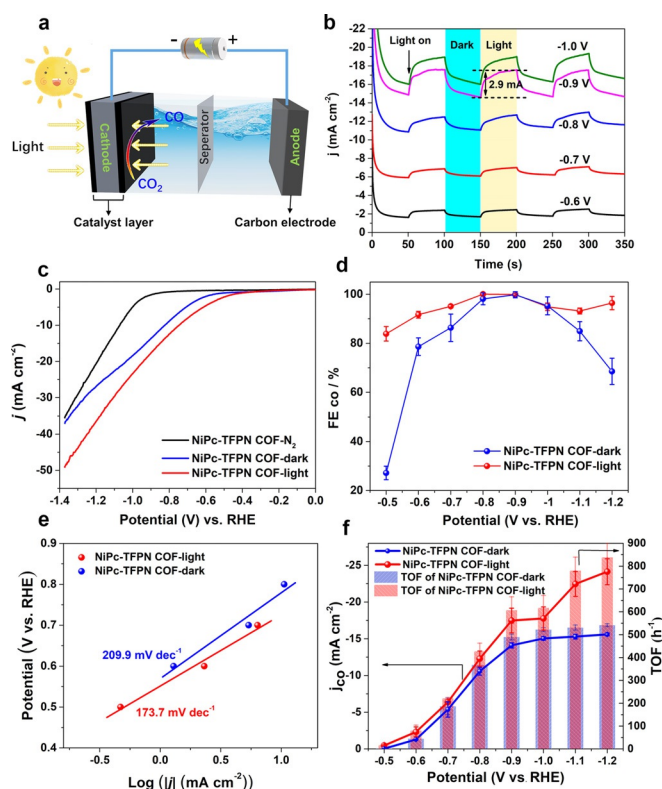
Tafel slopes were calculated to elucidate the dynamic activity of MPc-TFPN COF for ECR (Figure 3c). The results showed that the Tafel slope for NiPc-TFPN COF is 209.9 mV dec^{-1}, which is much smaller than that of CoPc-TFPN COF (570 mV dec^{-1}) and ZnPc-TFPN COF (230.9 mV dec^{-1}). This indicates that NiPc-TFPN COF has good CO_2 to CO kinetics, which may be attributed to the high initial electron transfer efficiency and large active surface during the catalytic process.[17] The electrochemical impedance spectroscopy (EIS) was also conducted to investigate the charge transfer resistance (Figure S37). The Nyquist plots demonstrated that NiPc-TFPN COF has much smaller charge transfer resistance than others due to its smallest semicircle in the high frequency region. We then calculated the partial current densities of CO (j_{CO}) and H_2 (j_{H_2}) at a wide range of potentials (Figure 3d). The results demonstrated that j_{CO} of NiPc-TFPN COF is larger than those of CoPc-TFPN COF at

−0.7 to 1.1 V, whilst at lower potentials ($< −0.7$ V), CoPc-TFPN COF performs better. According to the above experimental results, we can see that NiPc-TFPN COF's CO_2 to CO selectivity and current density are higher than CoPc-TFPN COF in a wide potential range, which leads us to the conclusion that NiPc-TFPN COF shows optimal performance for ECR among these COFs materials. This result is consistent with the results previously reported for NiPc or Ni-N_4 based catalysts.[7a,d,8c] Besides, the turnover frequency (TOF) of NiPc-TFPN COF was calculated to be 490 h^{-1} at −0.9 V, large than CoPc-TFPN COF(369 h^{-1} at −0.9 V).

Long-term stability remains a challenge for metallo-phthalocyanine based catalysts despite their effectiveness in the electroreduction of CO_2 to CO.[16a] Time-dependent total current density of NiPc-TFPN COF was first tested at wide potentials from −0.5 to −1.2 V. All of them remained stable during 1 h, suggesting the sufficient stability of the catalyst (Figures S38,39). Furthermore, we found NiPc/CoPc-TFPN COF catalysts can be continuously operated at least 60 h with well maintained current density of ≈ 16.3 mA cm^{-2}/ ≈ 12.1 mA cm^{-2} and a stable FE$_{CO}$ of 98.0–99.9 %/94.5–97 % in an H-cell at a constant potential of −0.9 V, suggesting their remarkable stability for long-term operations (Figure 3 e). In order to confirm that the produced CO indeed comes from the reduction of CO_2, the ^{13}C isotope labeling experiments were performed. When using $^{13}CO_2$ as substrates, ^{13}CO ($m/z =$ 29) was finally detected by using mass spectrometry, which confirmed that the produced CO originates from the reactant CO_2 instead of decomposition of catalysts (Figure S40).

Photo-coupled electrochemical CO_2 reduction activity of COFs

Phthalocyanine, as a photosensitive 18π aromatic macrocyclic compound, its electronic properties can be dramatically altered under light driving, thus may alter its intrinsic activity and energy efficiency.[11,18] Phthalocyanine moieties also possess efficient light absorption capabilities.[11,19] Besides, many previous works have proved that the light field effect plays an important role in electrocatalytic processes.[5,6b,20] In view of this, we proposed that light irradiation probably facilitates electrochemical activation of CO_2 molecule over phthalocyanine COFs catalyst. To verify this assumption, we carried out the PECR test for MPc-TFPN COF as shown in Figure 4 a. Before evaluating the PECR activity of these photo coupled electrocatalysts, we conducted a photo-current response test of the COFs material at different potentials in a CO_2 saturated 0.5 M KHCO$_3$ solution (NiPc-TFPN COF was taken as an example due to its strong light absorption capacity as shown in Figure S41, as well as its optimal ECR performance). The experiment results showed that the current density increases obviously under the trigger of light excitation (Figure 4 b). For comparison, we also tested the photo-current response of the NiPc-TFPN COF in an N_2-bubbling 0.5 M KHCO$_3$ solution, which only showed a very small photo-current response (Figure S42). The above results indicate that light excitation can indeed enhance the activation of CO_2, thus increasing the catalytic efficiency of electrocatalytic CO_2 reduction reaction.

Figure 4. Evaluation of CO_2 reduction performance of NiPc-TFPN COF by photo-coupled electrochemical measurements. a) Schematic of photo-coupled electrochemical measurements method. b) Photo-current response curve of NiPc-TFPN COF at different bias voltage in H-cell. c) The LSV curves of NiPc-TFPN COF under dark and light. d) FE$_{CO}$, e) Tafel plot of NiPc-TFPN COF under dark and light. f) j_{CO}, and TOF at different potentials under dark and light. The error bars represent the standard deviation of three independent measurements.

LSV curves were then tested and compared under dark and light conditions, respectively (Figure 4 c). The current density of NiPc-TFPN COF in N_2-saturated electrolyte (black curve) was relatively low but was far increased in CO_2-saturated electrolyte (blue curve), which proved that CO_2 participates in the reaction, that is, the ECR process occurs. More importantly, with the assistance of light (red curve), the current density of NiPc-TFPN COF was further improved obviously (increased from ≈ 14.1 to ≈ 17.5 mA cm^{-2} at −0.9 V, versus RHE). All the above results suggested that the ECR activity of the catalyst will be enhanced under light assistance. To further prove the above conclusion, the effect of light on FE at different potentials was also investigated. When coupled with light, the FE$_{CO}$ of NiPc-TFPN COF exhibited higher than 90 % in a wide potential range from −0.6 to −1.2 V and the maximum FE$_{CO}$ can reach up to almost 100 % at −0.8 V to −0.9 V (Figure 4 d), which is one of the highest among reported COFs (Table S1). In contrast, the potential range of when FE$_{CO} > 90$ % in the dark environment was only −0.8 to −1.0 V. Moreover, the results also indicated that the overpotential for the maximum FE$_{CO}$ has a positive shift about 0.1 V, implying that the photo-excited Ni-phthalocyanine COFs is beneficial to CO_2 reduction under relatively low potential. The photo-coupled ECR stability of

NiPc-TFPN COF was tested under light irradiation at −0.9 V vs. RHE, although its current density showed a very small decrease within 16 hours, which may be caused by photo corrosion or sample shedding; meanwhile, the FE_{CO} remained almost unchanged (Figure S43). The crystallinity and structural integrity of NiPc-TFPN COF were retained after the PECR reaction, as confirmed by PXRD, FTIR, and XPS characterizations (Figures S44–46). All of these confirmed that NiPc-TFPN COF materials are efficient and selective photo-coupled electrocatalyst for ECR.
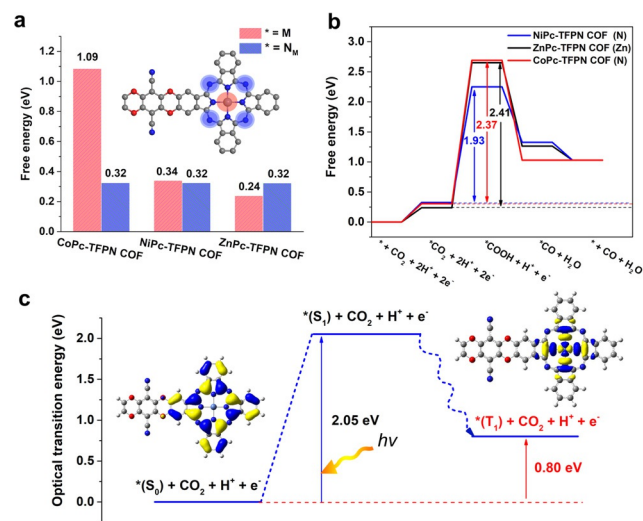
Tafel slopes were calculated to elucidate the catalytic kinetics of these electrocatalysts under dark and light environments, respectively. The results showed that the Tafel slope for NiPc-TFPN COF under light is 173.7 mV dec^{-1}, which is much smaller than that under dark (209.9 mV dec^{-1}) (Figure 4e). This value is higher than 118 mV dec^{-1}, suggesting that the adsorbed CO_2 receiving an electron and combining with H^+ from the electrolyte to form *COOH (the adsorbed $*CO_2 + [H^+ + e^-] \rightarrow *COOH$) is the rate determine step (RDS).[21] The Tafel slope drastically decreased under light indicated that external light-field can accelerate the electron transfer in phthalocyanine COFs.[5] To better investigate the effect of light irradiation on the catalytic active sites, we calculated the TOF and j_{CO} at different overpotentials (Figure 4f). These results showed that both TOF and j_{CO} are significantly enhanced in a wide potential range (−0.5 V to −1.2 V), and the activation effect by light irradiation was more obvious with the increase of overpotential. Based on the above experimental results, we can concluded that coupled with light can strongly enhance the ECR activity by interfering with the electron transfer characteristics of phthalocyanine COFs, which is conducive to the reduction of CO_2.

We further studied the effect of light irradiation on ECR activity of CoPc-TFPN COF and ZnPc-TFPN COF (Figures S47–54). The photo-current response test of the CoPc-TFPN COF and ZnPc-TFPN COF material at different potentials showed that the total current density also increases obviously under the trigger of light excitation. For CoPc-TFPN COF, the ECR test results show that when coupled with light, the FE_{CO} only exhibited slightly higher compared to the dark environment in the narrow potential range of −0.8 to −1.1 V vs. RHE. While for ZnPc-TFPN COF, the FE_{CO}, j_{CO} and TON all showed much higher than that measured under dark at all applied potentials, implying that the photo-excited phthalocyanine COFs is beneficial to CO_2 reduction. According to the ECR performance of these three kinds of COFs under light excitation, the following conclusions can be obtained: 1). For NiPc-TFPN COF and ZnPc-TFPN COF, the ECR performance of both of them were greatly improved in the relatively low overpotential range (from −0.5 to −0.7 V), while the performances of CoPc-TFPN COF were almost unchanged. Previous reports have shown that external light irradiation can facilitate internal electrons transfer for light sensitive catalysts[5] However, the Tafel plot test results imply that CoPc-TFPN COF has a very large Tafel slope (Figure S50), indicating that it has intrinsic low dynamic activity and low electron transfer efficiency. Hence, the effect of light excitation on its electron transfer is very limited, making it hardly to improve the performance under light

irradiation. However, at more negative potential (from −0.8 to −1.2 V), the j_{CO} and TOF are increased obviously, which indicates that the synergistic effect of high potential and photoexcited electrons are more significant, therefore accelerate the catalytic efficiency. 2). For the FE_{CO}, j_{CO} and TOF of ZnPc-TFPN COF, the general trend is that the performance peak position moves to more positive potential, confirming that external light-field can reduce the overpotential for CO_2 activation by affect electronic property of catalysts.

Investigating structure-property relationships

In view of the precise crystal structure of MPc-TFPN COF, we then studied its structure-property relationships for ECR by combining theoretical calculations with experiments. Among these elementary reaction steps, the adsorption of CO_2 on the MPc and then accompanied by a proton-coupled electron transfer step to generate *COOH was calculated to be the RDS for CO_2 to CO on MPc-TFPN COFs. DFT calculation results indicate that in our COFs system, the N atom in the Pc ligand plays an important role in adsorbing and activating CO_2. As for NiPc-TFPN COF and CoPc-TFPN COF, the free energy change for CO_2 adsorption on central metal is much higher than N site (N_M, which means N in MPc, which is highlighted with blue background in Figure 5a). Therefore, according to the minimum energy principle, CO_2 molecule tends to be adsorbed and activated on N_M atoms in the first step of ECR ($* + CO_2 + 2H^+ + 2e^- \rightarrow *CO_2 + 2H^+ + 2e^-$) on these two catalysts. While Zn atom on ZnPc-TFPN COF showed lower free energy change of CO_2 to $*CO_2$ compared to N site (N_{Zn}). Thus it is more reasonable that the first step of CO_2 activation is carried out on Zn atom for

Figure 5. Mechanism and DFT calculations. a) Comparison of the relative adsorption energy for first step of ECR ($* + CO_2 + 2H^+ + 2e^- \rightarrow *CO_2 + 2H^+ + 2e^-$) on metal site and nitrogen site on MPc-TFPN COF. b) The free energy diagrams for CO_2 reduction to CO on MPc-TFPN COF (Note that the symbol in brackets represent the reaction sites). The rate-determining step and the corresponding free energy on each COFs are indicated. c) Schematic representation of the excited states of NiPc-TFPN COF.

ZnPc-TFPN COF. The calculated Gibbs free energy diagram for CO_2 reduction processes on MPc-TFPN COF was shown in Figure 5b and S57–59. The calculated ΔG for NiPc-TFPN COF from adsorbed $*CO_2$ to $*COOH$ is lower than that of CoPc-TFPN COF and ZnPc-TFPN COF, indicating a higher CO_2 reduction activity, which is in line with our experimental results. We also studied the possible transfer process of $*COOH$ between metal and N in MPc during the reaction, as shown in Figures S60,61. However, these results indicate that transferring of $*COOH$ group from the metal center to the N atom of the MPc ligand is kinetically unfavorable because of the high activation energy barrier, see Supporting information for details.

In order to understand the effect of light on catalytic activity, the electronic properties of S_1 and T_1 excited states of these phthalocyanine COFs catalysts were calculated. After light irradiation, the NiPc-TFPN COF was first excited from S_0 to S_1 state and then spontaneously transformed to T_1 state through the process of intersystem crossing (Figure 5c). The energy gap between S_0 and S_1 is 2.05 eV, which is consistent with the band gap calculated from the measured UV-vis absorption spectrum, which also proved the accuracy of the calculation model systems. The optical transition energy of T_1 state is 0.80 eV (vs. ground state), indicating that under light conditions, the phthalocyanine COFs catalysts will be excited to a higher energy excited state. In addition to enhancing the electron transfer from the ligand to the active center, the COFs catalyst in the T_1 excited state is also more conducive to the activation of CO_2 to $*COOH$ due to the reduced free energy change compared to the ground state.[5] This explains the inherent reason why NiPc-TFPN COF performers better ECR activity under the irradiation of light.

Conclusion

In this work, a series of highly stable dioxin-linked metallophthalocyanine 2D-COFs were rationally designed. The crystal structure suggested that MPc-TFPN COF possesses highly uniformly dispersed single metal sites, which coordinate in the center of phthalocyanine, making these COFs ideal SSCs. At first, its performance for ECR was systematically studied, and the results showed that NiPc-TFPN COF and CoPc-TFPN COF exhibited superior activity and selectivity ($FE_{CO} = 99.8(\pm 1.24)\%$ for NiPc-TFPN COF and $96.1(\pm 1.25)\%$ for CoPc-TFPN COF at -0.9 V vs. RHE, respectively), also shown ultra-long cyclic stability (60 h). More importantly, by coupling with light, the j_{CO} and FE_{CO} further showed obvious enhancement compared to tested in the dark environment (j_{CO} increased from 14.1 to 17.5 mA cm^{-2} at -0.9 V. FE_{CO} reached up to $\approx 100\%$ at -0.8 to -0.9 V and the overpotential for the maximum FE_{CO} has a positive shift about 100 mV), indicating higher performance for PECR. Mechanism study revealed that external light-field can enhance the electron transfer to the adsorbed CO_2 in phthalocyanine COFs, which is conducive to the reduction of CO_2. This is the first report of dioxin-linked metallophthalocyanine COFs, which show excellent performance for ECR and PECR. Our results also highlight that external light irradiation has a significant effect on the ECR activity and product selectivity for light-sensitive electrocatalysts.

Conflict of interest

The authors declare no conflict of interest.

[1] a) S. Solomon, G.-K. Plattner, R. Knutti, P. Friedlingstein, *Proc. Natl. Acad. Sci. USA* **2009**, *106*, 1704; b) S. J. Davis, K. Caldeira, H. D. Matthews, *Science* **2010**, *329*, 1330; c) B. Obama, *Science* **2017**, *355*, 126.

[2] a) P. De Luna, R. Quintero-Bermudez, C.-T. Dinh, M. B. Ross, O. S. Bushuyev, P. Todorović, T. Regier, S. O. Kelley, P. Yang, E. H. Sargent, *Nat. Catal.* **2018**, *1*, 103–110; b) P. De Luna, C. Hahn, D. Higgins, S. A. Jaffer, T. F. Jaramillo, E. H. Sargent, *Science* **2019**, *364*, eaav3506.

[3] a) J. Qiao, Y. Liu, F. Hong, J. Zhang, *Chem. Soc. Rev.* **2014**, *43*, 631–675; b) S. Lin, C. S. Diercks, Y.-B. Zhang, N. Kornienko, E. M. Nichols, Y. Zhao, A. R. Paris, D. Kim, P. Yang, O. M. Yaghi, C. J. Chang, *Science* **2015**, *349*, 1208; c) A. S. Varela, N. Ranjbar Sahraie, J. Steinberg, W. Ju, H.-S. Oh, P. Strasser, *Angew. Chem. Int. Ed.* **2015**, *54*, 10758–10762; *Angew. Chem.* **2015**, *127*, 10908–10912.

[4] a) D. Yang, B. Ni, X. Wang, *Adv. Energy Mater.* **2020**, *10*, 2001142; b) X. Huang, Q. Shen, J. Liu, N. Yang, G. Zhao, *Energy Environ. Sci.* **2016**, *9*, 3161–3171.

[5] D. Yang, H. Yu, T. He, S. Zuo, X. Liu, H. Yang, B. Ni, H. Li, L. Gu, D. Wang, X. Wang, *Nat. Commun.* **2019**, *10*, 3844.

[6] a) B. Zhou, X. Kong, S. Vanka, S. Cheng, N. Pant, S. Chu, P. Ghamari, Y. Wang, G. Botton, H. Cuo, Z. Mi, *Energy Environ. Sci.* **2019**, *12*, 2842–2848; b) X. Deng, R. Li, S. Wu, L. Wang, J. Hu, J. Ma, W. Jiang, N. Zhang, X. Zheng, C. Gao, L. Wang, Q. Zhang, J. Zhu, Y. Xiong, *J. Am. Chem. Soc.* **2019**, *141*, 10924–10929.

[7] a) W. Ju, A. Bagger, G.-P. Hao, A. S. Varela, I. Sinev, V. Bon, B. Roldan Cuenya, S. Kaskel, J. Rossmeisl, P. Strasser, *Nat. Commun.* **2017**, *8*, 944; b) X. Zhang, Z. Wu, X. Zhang, L. Li, Y. Li, H. Xu, X. Li, X. Yu, Z. Zhang, Y. Liang, H. Wang, *Nat. Commun.* **2017**, *8*, 14675; c) X. Li, W. Bi, M. Chen, Y. Sun, H. Ju, W. Yan, J. Zhu, X. Wu, W. Chu, C. Wu, Y. Xie, *J. Am. Chem. Soc.*

4870   www.angewandte.org

© 2020 Wiley-VCH GmbH

Angew. Chem. Int. Ed. **2021**, *60*, 4864–4871

2017, *139*, 14889 – 14892; d) S. Liu, H. B. Yang, S.-F. Hung, J. Ding, W. Cai, L. Liu, J. Gao, X. Li, X. Ren, Z. Kuang, Y. Huang, T. Zhang, B. Liu, *Angew. Chem. Int. Ed.* **2020**, *59*, 798 – 803; *Angew. Chem.* **2020**, *132*, 808 – 813.

[8] a) M. Wang, K. Torbensen, D. Salvatore, S. Ren, D. Joulié, F. Dumoulin, D. Mendoza, B. Lassalle-Kaiser, U. Işci, C. P. Berlinguette, M. Robert, *Nat. Commun.* **2019**, *10*, 3602; b) X. Zhang, Z. Wu, X. Zhang, L. Li, Y. Li, H. Xu, X. Li, X. Yu, Z. Zhang, Y. Liang, H. Wang, *Nat. Commun.* **2017**, *8*, 14675; c) X. Zhang, Y. Wang, M. Gu, M. Wang, Z. Zhang, W. Pan, Z. Jiang, H. Zheng, M. Lucero, H. Wang, G. E. Sterbinsky, Q. Ma, Y.-G. Wang, Z. Feng, J. Li, H. Dai, Y. Liang, *Nat. Energy* **2020**, *5*, 684 – 692.

[9] C. S. Diercks, Y. Liu, K. E. Cordova, O. M. Yaghi, *Nat. Mater.* **2018**, *17*, 301 – 307.

[10] a) X. Chen, K. Geng, R. Liu, K. T. Tan, Y. Gong, Z. Li, S. Tao, Q. Jiang, D. Jiang, *Angew. Chem. Int. Ed.* **2020**, *59*, 5050 – 5091; *Angew. Chem.* **2020**, *132*, 5086 – 5129; b) K. Geng, T. He, R. Liu, K. T. Tan, Z. Li, S. Tao, Y. Gong, Q. Jiang, D. Jiang, *Chem. Rev.* **2020**, *120*, 8814 – 8933.

[11] G. de la Torre, C. G. Claessens, T. Torres, *Chem. Commun.* **2007**, 2000 – 2015.

[12] a) X. Guan, H. Li, Y. Ma, M. Xue, Q. Fang, Y. Yan, V. Valtchev, S. Qiu, *Nat. Chem.* **2019**, *11*, 587 – 594; b) B. Zhang, M. Wei, H. Mao, X. Pei, S. A. Alshmimri, J. A. Reimer, O. M. Yaghi, *J. Am. Chem. Soc.* **2018**, *140*, 12715 – 12719.

[13] a) E. L. Spitler, W. R. Dichtel, *Nat. Chem.* **2010**, *2*, 672 – 677; b) X. Ding, J. Guo, X. Feng, Y. Honsho, J. Guo, S. Seki, P. Maitarad, A. Saeki, S. Nagase, D. Jiang, *Angew. Chem. Int. Ed.* **2011**, *50*, 1289 – 1293; *Angew. Chem.* **2011**, *123*, 1325 – 1329; c) E. L. Spitler, J. W. Colson, F. J. Uribe-Romo, A. R. Woll, M. R. Giovino, A. Saldivar, W. R. Dichtel, *Angew. Chem. Int. Ed.* **2012**, *51*, 2623 – 2627; *Angew. Chem.* **2012**, *124*, 2677 – 2681; d) S. Jin, X. Ding, X. Feng, M. Supur, K. Furukawa, S. Takahashi, M. Addicoat, M. E. El-Khouly, T. Nakamura, S. Irle, S. Fukuzumi, A. Nagai, D. Jiang, *Angew. Chem. Int. Ed.* **2013**, *52*, 2017 – 2021; *Angew. Chem.* **2013**, *125*, 2071 – 2075; e) S. Jin, M. Supur, M. Addicoat, K. Furukawa, L. Chen, T. Nakamura, S. Fukuzumi, S. Irle, D. Jiang, *J. Am. Chem. Soc.* **2015**, *137*, 7817 – 7827; f) Z. Meng, R. M. Stolz, K. A. Mirica, *J. Am. Chem. Soc.* **2019**, *141*, 11929 – 11937; g) M. Wang, M. Ballabio, M. Wang, H.-H. Lin, B. P. Biswal, X. Han, S. Paasch, E. Brunner, P. Liu, M. Chen, M. Bonn, T. Heine, S. Zhou, E. Cánovas, R. Dong, X. Feng, *J. Am. Chem. Soc.* **2019**, *141*, 16810 – 16816.

[14] a) W. Zhong, R. Sa, L. Li, Y. He, L. Li, J. Bi, Z. Zhuang, Y. Yu, Z. Zou, *J. Am. Chem. Soc.* **2019**, *141*, 7615 – 7621; b) Y. Zeng, R.

Zou, Y. Zhao, *Adv. Mater.* **2016**, *28*, 3032 – 3032; c) W. Zhou, Q.-W. Deng, G.-Q. Ren, L. Sun, L. Yang, Y.-M. Li, D. Zhai, Y.-H. Zhou, W.-Q. Deng, *Nat. Commun.* **2020**, *11*, 4481; d) C.-L. Yao, J.-C. Li, W. Gao, Q. Jiang, *Chem. Eur. J.* **2018**, *24*, 11051 – 11058.

[15] J. Jiao, R. Lin, S. Liu, W.-C. Cheong, C. Zhang, Z. Chen, Y. Pan, J. Tang, K. Wu, S.-F. Hung, H. M. Chen, L. Zheng, Q. Lu, X. Yang, B. Xu, H. Xiao, J. Li, D. Wang, Q. Peng, C. Chen, Y. Li, *Nat. Chem.* **2019**, *11*, 222 – 228.

[16] a) N. Han, Y. Wang, L. Ma, J. Wen, J. Li, H. Zheng, K. Nie, X. Wang, F. Zhao, Y. Li, J. Fan, J. Zhong, T. Wu, D. J. Miller, J. Lu, S.-T. Lee, Y. Li, *Chem* **2017**, *3*, 652 – 664; b) N. Morlanés, K. Takanabe, V. Rodionov, *ACS Catal.* **2016**, *6*, 3092 – 3095; c) W. W. Kramer, C. C. L. McCrory, *Chem. Sci.* **2016**, *7*, 2506 – 2515; d) N. Huang, K. H. Lee, Y. Yue, X. Xu, S. Irle, Q. Jiang, D. Jiang, *Angew. Chem. Int. Ed.* **2020**, *59*, 16587 – 16593; *Angew. Chem.* **2020**, *132*, 16730 – 16736.

[17] a) Y. R. Wang, Q. Huang, C. T. He, Y. Chen, J. Liu, F. C. Shen, Y. Q. Lan, *Nat. Commun.* **2018**, *9*, 4466; b) H.-J. Zhu, M. Lu, Y.-R. Wang, S.-J. Yao, M. Zhang, Y.-H. Kan, J. Liu, Y. Chen, S.-L. Li, Y.-Q. Lan, *Nat. Commun.* **2020**, *11*, 497.

[18] J. Bian, J. Feng, Z. Zhang, Z. Li, Y. Zhang, Y. Liu, S. Ali, Y. Qu, L. Bai, J. Xie, D. Tang, X. Li, F. Bai, J. Tang, L. Jing, *Angew. Chem. Int. Ed.* **2019**, *58*, 10873 – 10878; *Angew. Chem.* **2019**, *131*, 10989 – 10994.

[19] a) X. Zhang, T. Peng, L. Yu, R. Li, Q. Li, Z. Li, *ACS Catal.* **2015**, *5*, 504 – 510; b) M.-E. Ragoussi, J.-J. Cid, J.-H. Yum, G. de la Torre, D. Di Censo, M. Grätzel, M. K. Nazeeruddin, T. Torres, *Angew. Chem. Int. Ed.* **2012**, *51*, 4375 – 4378; *Angew. Chem.* **2012**, *124*, 4451 – 4454; c) X. Zhang, L. Yu, C. Zhuang, T. Peng, R. Li, X. Li, *ACS Catal.* **2014**, *4*, 162 – 170.

[20] a) M. Schreier, F. Héroguel, L. Steier, S. Ahmad, J. S. Luterbacher, M. T. Mayer, J. Luo, M. Grätzel, *Nat. Energy* **2017**, *2*, 17087; b) T. G. Ulusoy Ghobadi, A. Ghobadi, M. Buyuktemiz, E. A. Yildiz, D. Berna Yildiz, H. G. Yaglioglu, Y. Dede, E. Ozbay, F. Karadas, *Angew. Chem. Int. Ed.* **2020**, *59*, 4082 – 4090; *Angew. Chem.* **2020**, *132*, 4111 – 4119.

[21] J.-H. Zhou, K. Yuan, L. Zhou, Y. Guo, M.-Y. Luo, X.-Y. Guo, Q.-Y. Meng, Y.-W. Zhang, *Angew. Chem. Int. Ed.* **2019**, *58*, 14197 – 14201; *Angew. Chem.* **2019**, *131*, 14335 – 14339.